Published online: October 26, 2017

Article

SOURCE DATA | TRANSPARENT PROCESS

THE EMBO JOURNAL

Human THO–Sin3A interaction reveals new mechanisms to prevent R-loops that cause genome instability

Irene Salas-Armenteros, Carmen Pérez-Calero, Aleix Bayona-Feliu, Emanuela Tumini, Rosa Luna* & Andrés Aguilera**

Abstract

R-loops, formed by co-transcriptional DNA–RNA hybrids and a displaced DNA single strand (ssDNA), fulfill certain positive regulatory roles but are also a source of genomic instability. One key cellular mechanism to prevent R-loop accumulation centers on the conserved THO/TREX complex, an RNA-binding factor involved in transcription elongation and RNA export that contributes to messenger ribonucleoprotein (mRNP) assembly, but whose precise function is still unclear. To understand how THO restrains harmful R-loops, we searched for new THO-interacting factors. We found that human THO interacts with the Sin3A histone deacetylase complex to suppress co-transcriptional R-loops, DNA damage, and replication impairment. Functional analyses show that histone hypo-acetylation prevents accumulation of harmful R-loops and RNA-mediated genomic instability. Diminished histone deacetylase activity in THO- and Sin3A-depleted cell lines correlates with increased R-loop formation, genomic instability, and replication fork stalling. Our study thus uncovers physical and functional crosstalk between RNA-binding factors and chromatin modifiers with a major role in preventing R-loop formation and RNA-mediated genome instability.

Keywords DNA–RNA hybrids; genome instability; histone acetylation; Sin3A deacetylase; THO/TREX

Subject Categories Chromatin, Epigenetics, Genomics & Functional Genomics; DNA Replication, Repair & Recombination; RNA Biology

DOI 10.15252/embj.201797208 | Received 24 April 2017 | Revised 22 September 2017 | Accepted 28 September 2017 | Published online 26 October 2017

The EMBO Journal (2017) 36: 3532–3547

Introduction

R-loops are nucleic acid structures that can form in cells and may have positive roles, for example, in immunoglobulin class switch recombination and in some cases of transcription activation or termination (Santos-Pereira & Aguilera, 2015) (Skourti-Stathaki & Proudfoot, 2014; Sollier & Cimprich, 2015). However, accumulating evidence shows that R-loops are a major threat to genome integrity, as first observed in yeast THO complex mutants (Huertas & Aguilera, 2003). This is largely due to the capacity of R-loops to halt replication and subsequently cause DNA breaks (Hamperl & Cimprich, 2014; Garcia-Muse & Aguilera, 2016). As a consequence, even though R-loops have been observed at different regions of the eukaryotic genome (Ginno *et al*, 2013; Wahba *et al*, 2016), cells have evolved factors and mechanisms to prevent harmful R-loop accumulation. THO is a conserved eukaryotic RNA-binding and RNA-processing/export complex required for R-loop prevention (Chavez *et al*, 2000; Huertas & Aguilera, 2003). Yeast and human cells lacking functional THO show strong transcription- and R-loop-dependent genome instability phenotypes that correlate with altered replication fork progression (Wellinger *et al*, 2006; Dominguez-Sanchez *et al*, 2011). A similar effect has also been shown for other factors related to RNA processing, such as SRSF1 (serine/arginine splicing factor 1), SETX/Sen1, DDX19, or DDX23 among others (Li & Manley, 2005; Paulsen *et al*, 2009; Tuduri *et al*, 2009; Skourti-Stathaki *et al*, 2011; Wahba *et al*, 2011; Stirling *et al*, 2012; Hodroj *et al*, 2017; Sridhara *et al*, 2017).

The involvement of RNA-binding and RNA-processing factors in preventing R-loop accumulation suggests that a suboptimal mRNP particle has a higher chance to bind back to the DNA template during transcription (Aguilera, 2005), a hypothesis supported by the fact that overexpression of specific RNA-binding proteins suppress the phenotypes of yeast THO mutants or SRSF1-depleted human cells (Jimeno *et al*, 2006; Li *et al*, 2007). Nevertheless, whether this is sufficient to explain how specific RNA binding factors control co-transcriptional accumulation of harmful R-loops is unclear. R-loops accumulate in normal cells and cause genome instability in cells lacking RNA-processing and export factors (Huertas & Aguilera, 2003; Hodroj *et al*, 2017; Li & Manley, 2005; Paulsen *et al*, 2009; Tuduri *et al*, 2009; Skourti-Stathaki *et al*, 2011; Wahba *et al*, 2011; Stirling *et al*, 2012; Sridhara *et al*, 2017), DNA repair factors such as BRCA2, BRCA1, and Fanconi anemia proteins

Centro Andaluz de Biología Molecular y Medicina Regenerativa-CABIMER, Consejo Superior de Investigaciones Científicas-Universidad Pablo de Olavide-Universidad de Sevilla, Seville, Spain

*Corresponding author. Tel: +34 954468374; E-mail: rlvaro@us.es

**Corresponding author. Tel: +34 954468372; E-mail: aguilo@us.es

(Bhatia *et al*, 2014; Garcia-Rubio *et al*, 2015; Hatchi *et al*, 2015; Schwab *et al*, 2015), or chromatin remodelers such as FACT (Herrera-Moyano *et al*, 2014), suggesting that R-loop dynamics are tightly controlled in cells.

DNA–RNA hybrids have been shown to be a replication obstacle (Wellinger *et al*, 2006; Gan *et al*, 2011; Madireddy *et al*, 2016). In the last years, it has been reported that DNA replication-associated activities, such as those of topoisomerases, MCM2-7 replicative helicase, and Fanconi anemia proteins, are necessary to prevent transcription–replication conflicts and R-loop accumulation (Tuduri *et al*, 2009; Garcia-Rubio *et al*, 2015; Schwab *et al*, 2015; Madireddy *et al*, 2016; Vijayraghavan *et al*, 2016). Since R-loops may constitute a major source of replication stress and genome instability (Garcia-Muse & Aguilera, 2016), a hallmark of tumor cells (Halazonetis *et al*, 2008), deciphering how cells prevent R-loop accumulation is crucial to understand the origin of genome instability.

To understand how RNA binding factors could protect genome integrity during transcription, we searched for new human proteins interacting with THO, an RNA binding factor with a primary role in transcription and mRNA processing and export that at the same time protects genome integrity by preventing R-loop formation (Luna *et al*, 2012). Interestingly, we provide evidence that THO "talks" to a repressive chromatin modifier, the Sin3A histone deacetylase complex. Various molecular and cellular analyses of Sin3A-depleted human cells and treatment with different chemical inhibitors of histone acetylation and deacetylation show that R-loops as well as transcription and R-loop-dependent genome instability are prevented by the Sin3A complex and by histone deacetylation. Our data suggest that specific co-transcriptional RNA binding factors, such as THO, may play a key role in promoting a local and transient chromatin closing after the passage of the RNA polymerase, to prevent harmful DNA–RNA interactions that lead to replication fork stalling and genome instability. This not only opens new perspectives to understand how cells prevent transcription-associated genome instability, but also suggests that the state of the nascent RNA may have a key role in chromatin remodeling and in modulating replication fork progression.

Results

The human Sin3A deacetylase complex interacts physically with THOC1

To gain insight into the mechanism by which specific RNA binding factors control R-loop accumulation, we searched for factors interacting with THO by yeast two-hybrid screening using as bait the THO subunit THOC1 and as prey a human cDNA library (Mate&Plate Library Universal Human-normalized; see Materials and Methods) (Fig EV1A). We obtained two clones, one containing a 1.6-kb fragment encoding 180 C-terminal amino acids (aa) of the 1,083-aa-protein SAP130 (Sin3A-associated protein 130), a subunit of the Sin3A histone deacetylase complex (HDAC) (Fleischer *et al*, 2003), and another containing a 1.1-kb fragment encoding 150 C-terminal amino acids of the 439-aa MFAP1 protein (microfibrillar-associated protein 1), implicated in mRNA splicing in *Drosophila* (Andersen & Tapon, 2008; Fig EV1A), and found in a global screening to interact with other human splicing factors (Hegele *et al*, 2012). In this study, we therefore focused on SAP130.

SAP130–THOC1 interaction was validated in human cells by co-immunoprecipitation (co-IP) with anti-SAP130 and anti-THOC1 antibodies (Fig 1A, upper panel) and by proximity ligation assay (PLA), which detects cellular protein–protein association *in situ* (Fig 1A, lower panel). Since SAP130 is a subunit of the conserved Sin3A histone deacetylase complex, we wondered whether THOC1 interacted with other components of the Sin3A complex. Notably, we found an *in vivo* interaction between THOC1 and SIN3, the core component that acts as the scaffold of the Sin3A complex, by co-IP experiments with anti-SIN3 and anti-THOC1 antibodies (Fig 1B, upper panel) and by PLA assays (Fig 1B, lower panel). The observation that THOC1 associates with SIN3 supports that THO and Sin3A complexes physically interact *in vivo*.

Sin3A depletion leads to transcription- and R-loop-dependent genome instability

To determine whether the physical interaction of the two complexes had any functional implication, we assayed whether SAP130 plays any role in the maintenance of genome integrity, as is the case of THOC1. Cells depleted of SAP130 by short interfering RNA (siRNA) showed a reduced growth rate, but no significant effect on cell cycle progression and apoptosis was observed (Fig EV1B–F). Then, we assayed the levels of DNA damage by single-cell electrophoresis (comet assays) in cells depleted of different subunits of the Sin3A complex, including SAP130, the scaffold subunit SIN3, SAP30, which acts as a bridge to other co-repressors, and SUDS3, required for the integrity and activity of the complex (Grzenda *et al*, 2009). Alkaline and neutral comet assays (Figs 2A and EV2A and B) revealed a significant increase in DNA breaks after depletion of the Sin3A subunits tested, although to a different degree, likely due to a varied physiological importance of the subunits. These results indicate that the Sin3A complex prevents DNA breaks similar to THO (Dominguez-Sanchez *et al*, 2011; Fig EV2B), and from now on we focused our study on the originally selected SAP130 and the scaffold subunit SIN3, as representative of the Sin3A complex and whose yeast orthologue Sin3 has been shown to suppresses R-loop-dependent genome instability (Wahba *et al*, 2011).

Next, we wondered whether, as shown for siTHO cells (Dominguez-Sanchez *et al*, 2011), DNA break accumulation in Sin3A-depleted cells was also dependent on transcription and RNA–DNA hybrids. DNA breaks were determined by single-cell electrophoresis (comet assay) in cells incubated with either cordycepin, an inhibitor of RNA chain elongation, or with the transcription inhibitor 5,6-dichloro-1-ß-D-ribofurosylbenzimidazole (DRB). At the concentrations used, both cordycepin and DRB inhibited transcription as determined by ethynyl uridine (EU) incorporation (Fig 2B and C, left panels), but did not significantly perturb the cycle progression as shown by FACS analysis (Fig EV2C). Cordycepin and DRB fully suppressed the increase in DNA breaks of SAP130 and SIN3 knock-down cells (Fig 2B and C, right panels), indicating that the effect is not specific of the inhibitors and that genome instability induced by depletion of these factors is mediated by transcription. Importantly, overexpression of RNase H1, a ribonuclease that specifically degrades the RNA moiety of

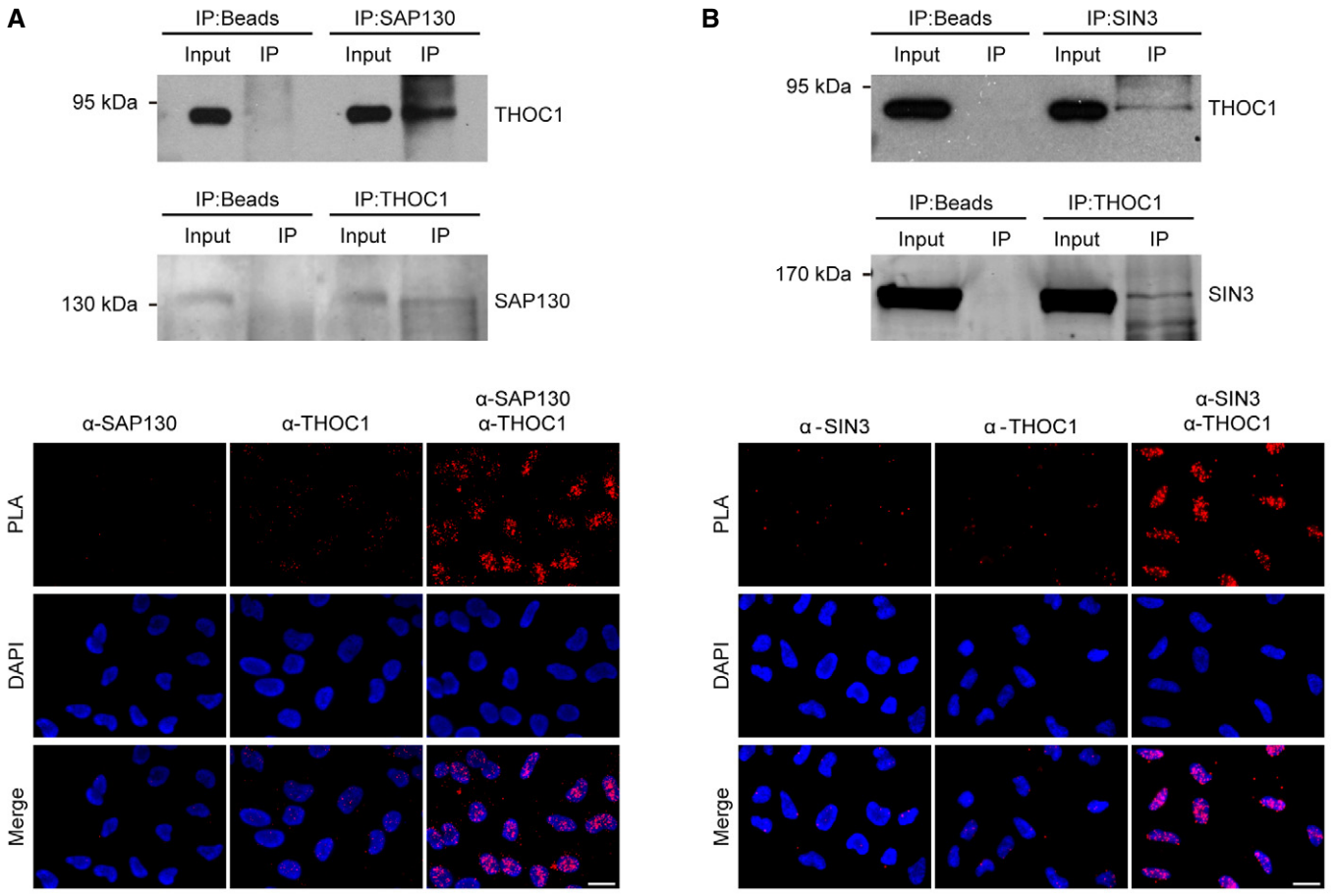

Figure 1. Human THOC1 physically interacts with the Sin3A deacetylase complex.

A THOC1 interaction with SAP130 detected by co-IP assays in whole-cell extracts of HEK293T with anti-SAP130 antibody and with anti-THOC1. Input extract and total immunoprecipitate (IP) were analyzed by Western blot with anti-THOC1 antibody and anti-SAP130, respectively (upper panel). Proximity ligation assay (PLA) in HeLa cells showing specific association of THOC1 and SAP130 endogenous proteins (lower panel). PLA signals (red spots) (n = 2).

B THOC1 interaction with SIN3 detected by co-IP assays in whole-cell extracts of HEK293T with anti-SIN3 antibody and with anti-THOC1. Input extract and total immunoprecipitate (IP) were analyzed by Western blot with anti-THOC1 antibody and anti-SIN3, respectively (upper panel). PLA showing association of THOC1 and SIN3 endogenous proteins (lower panel) (n = 2).

Data information: Input lanes represent 1% of the amount of whole-cell extract used in each experiment. Scale bars, 20 μm.
Source data are available online for this figure.

RNA–DNA hybrids, completely suppressed the accumulation of DNA breaks in SIN3 and SAP130 knock-down cells, as determined by alkaline comet assays (Fig 2D).

Consequently, we assayed whether or not R-loops were increased in SAP130 and SIN3 knock-down cells by immunofluorescence (IF) using the anti-RNA–DNA hybrid S9.6 monoclonal antibody. A significant enrichment of the S9.6 nuclear signal was observed in both SAP130- and SIN3-depleted cells as well as in THOC1-depleted cells, included as a positive control (Figs 3 and EV3A). Importantly, this increase was suppressed by RNaseH1 overexpression, which normalized the S9.6 signal in SAL30/SIN3 knock-down cells to that of control cells, confirming the enrichment of the R-loop signal in the siRNA-treated cells (Fig 3). The increase in background S9.6 signal intensity observed in control cells expressing RNAse H1 is likely due to the stress caused by RNaseH1 overexpression, which can increase the levels of DNA damage and replicative stress (Paulsen *et al*, 2009; Dominguez-Sanchez *et al*, 2011). S9.6 nucleolar signal was also increased after depletion of SIN3, in agreement with an enhanced hybrid formation at ribosomal DNA in yeast mutants (Wahba *et al*, 2011) and in THOC1-depleted cells (Fig EV3B). Next, we assayed whether we could also detect an increase in R-loop accumulation at the molecular level by DRIP-qPCR using the S9.6 monoclonal antibody in four human genes (*APOE*, *RPL13A*, *BTBD19,* and *EGR1*) that have been previously validated for R-loop detection (Ginno *et al*, 2013; Herrera-Moyano *et al*, 2014). Specific immunoprecipitation of DNA–RNA hybrids was confirmed by *in vitro* treatment with RNase H. Results clearly show higher levels of RNA–DNA hybrids in SAP130- and SIN3-depleted than in control RNAi cells (Figs 4A and EV3C). A more extensive analysis of the *RPL13A* gene, exhibiting high levels of RNA–DNA hybrids in SAP130 and SIN3 knock-down cells, revealed R-loop accumulation in all regions tested, from 5′ to 3′ ends, in agreement with Sin3A's role in preventing co-transcriptional R-loops along the gene (Figs 4B and EV3D). These high levels of RNA–DNA hybrids

Published online: October 26, 2017

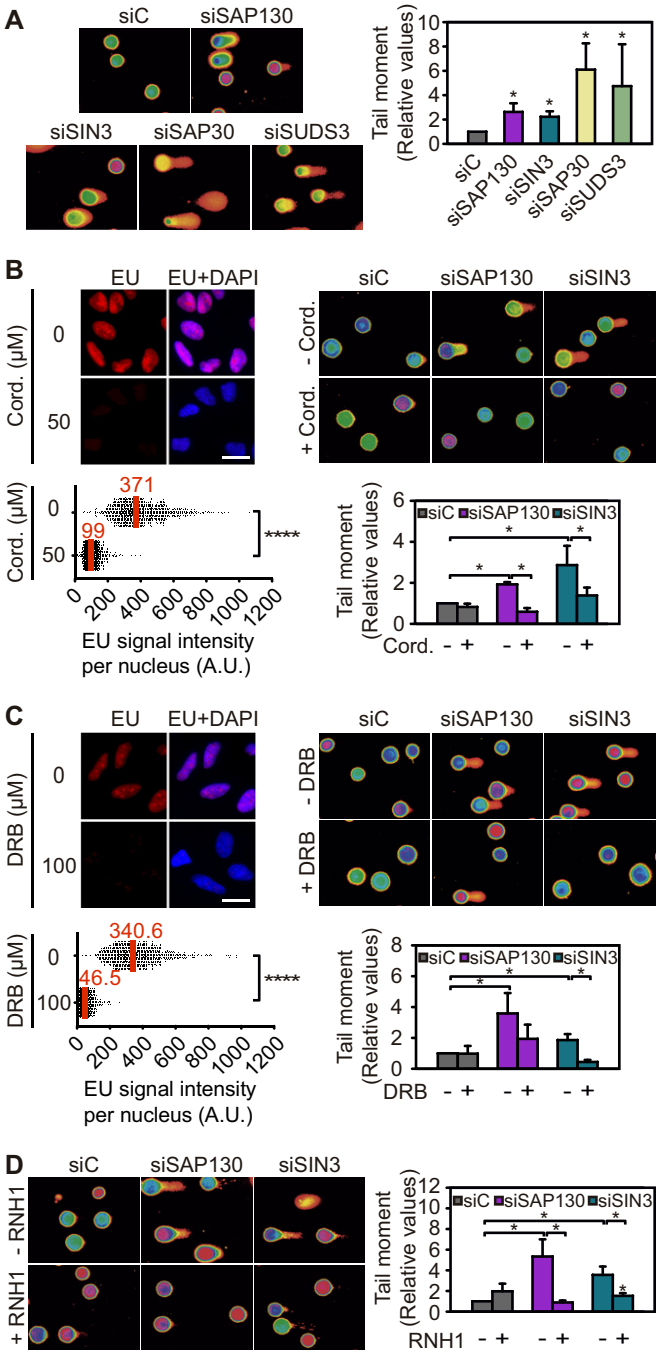

Figure 2. Sin3A complex-depletion leads to DNA breaks that are dependent on transcription and R-loops.

A Alkaline single-cell electrophoresis in siC- (control), siSAP130-, siSIN3-, siSAP30-, and siSUDS3-transfected HeLa cells. Data are plotted as mean ± SEM (n = 3).

B EU labeling in HeLa cells untreated or treated for 4 h with 50 μM cordycepin (left panel). The median of the EU signal intensity per nucleus is shown (n = 3). Comet assays in HeLa cells transfected with siC, siSAP130, or siSIN3 untreated or treated with cordycepin (right panel). Data are plotted as mean ± SEM (n = 3).

C EU labeling in HeLa cells untreated or treated for 4 h with 100 μM DRB (left panel). The median of the EU signal intensity per nucleus is shown (n = 3). Comet assays in HeLa cells transfected with siC, siSAP130, or siSIN3 untreated or treated with DRB (right panel). Data are plotted as mean ± SEM (n = 3).

D Comet assays in siC, siSAP130, and siSIN3 cells transfected with pcDNA3 (−RNH1) or pcDNA3-RNaseH1 (+RNH1) for 48 h. Data are plotted as mean ± SEM (n = 3).

Data information: For EU incorporation assays in (B, C), around 900 cells from three independent experiments were considered; ****P < 0.0001 (Mann–Whitney U-test, two-tailed). Scale bars, 20 μm. For comet assays in (A–D), more than 100 cells were counted in each of the three experiments; *P < 0.05 (Mann–Whitney U-test).

were not due to an increase in transcription, since no significant differences in mRNA levels, as detected by RT–qPCR, or in RNAPII occupancy, as determined by ChIP analyses, were observed (Fig EV3E). Interestingly, double depletion of THO and Sin3A conferred a significant increase in R-loops, as determined by S9.6 IF assays, not only compared to control cells but also to cells depleted of each factor individually (Figs 5A and B, and EV4A). R-loop accumulation in double siRNA-treated cells was confirmed by RNaseH1 overexpression (Fig 5A) and also by DRIP analysis (Figs 5C and EV4B and C). Altogether, the results support a functional interaction between Sin3A complex and THO to prevent R-loop formation.

Histones are hyper-acetylated in THOC1-depleted cells

Since histone hyper-acetylation facilitates an open chromatin (Shahbazian & Grunstein, 2007), it is likely that it promotes R-loop formation. Therefore, we reasoned that THO could interact with Sin3A to transiently promote histone deacetylation as a way to transiently close chromatin, thus preventing the nascent RNA to hybridize with the DNA template. For this reason, we determined by ChIP whether Sin3A recruitment to R-loop-accumulating genes was defective in THOC1 knock-down cells. No differences were observed with respect to the siRNA control (Fig EV4D). To test whether histone acetylation was impaired in THOC1-depleted cells, we determined global histone acetylation by Western blotting. Utilizing an antibody that recognizes various histone-acetylated residues, histones H3 and H4 acetylation levels in THOC1-depleted cells were found similar to those of Sin3A-depleted cells and slightly increased with respect to the acetylation levels of control RNAi cells (Fig 6A). When specific antibodies were used, a slight increase in specific marks such as H3K14 acetylation was also detected (Fig EV4E). Given that global histone acetylation levels are increased in both Sin3A- and THO-depleted cells (Fig 6A), we performed ChIP analysis with antibodies that recognized various histone-acetylated residues at loci that accumulated R-loops, as determined by DRIP. ChIP data indicate a slight increase in histone acetylation at some of loci but not others (Fig 6B). The lack of significant difference in the ChIP signals, even in cells depleted of Sin3A, may be explained because this antibody detects globally acetylated histone H3 and not specific residues. Since the residue(s) deacetylated by Sin3A are still unclear, we used an alternative strategy to address whether THO–Sin3A interaction could influence histone deacetylation as the Western blot data suggest (Fig 6A). To test this possibility, we measured the histone deacetylase activity of THOC1- and SIN3-depleted cells by fluorimetric assays (Fig 6C). HDAC activity was reduced in both THOC1 and SIN3 knock-down cells, and no synergistic effect was observed in double-depleted cells (Fig 6C). These results, therefore, suggest that both THO and Sin3A modulate co-transcriptional histone acetylation levels.

Published online: October 26, 2017
The EMBO Journal

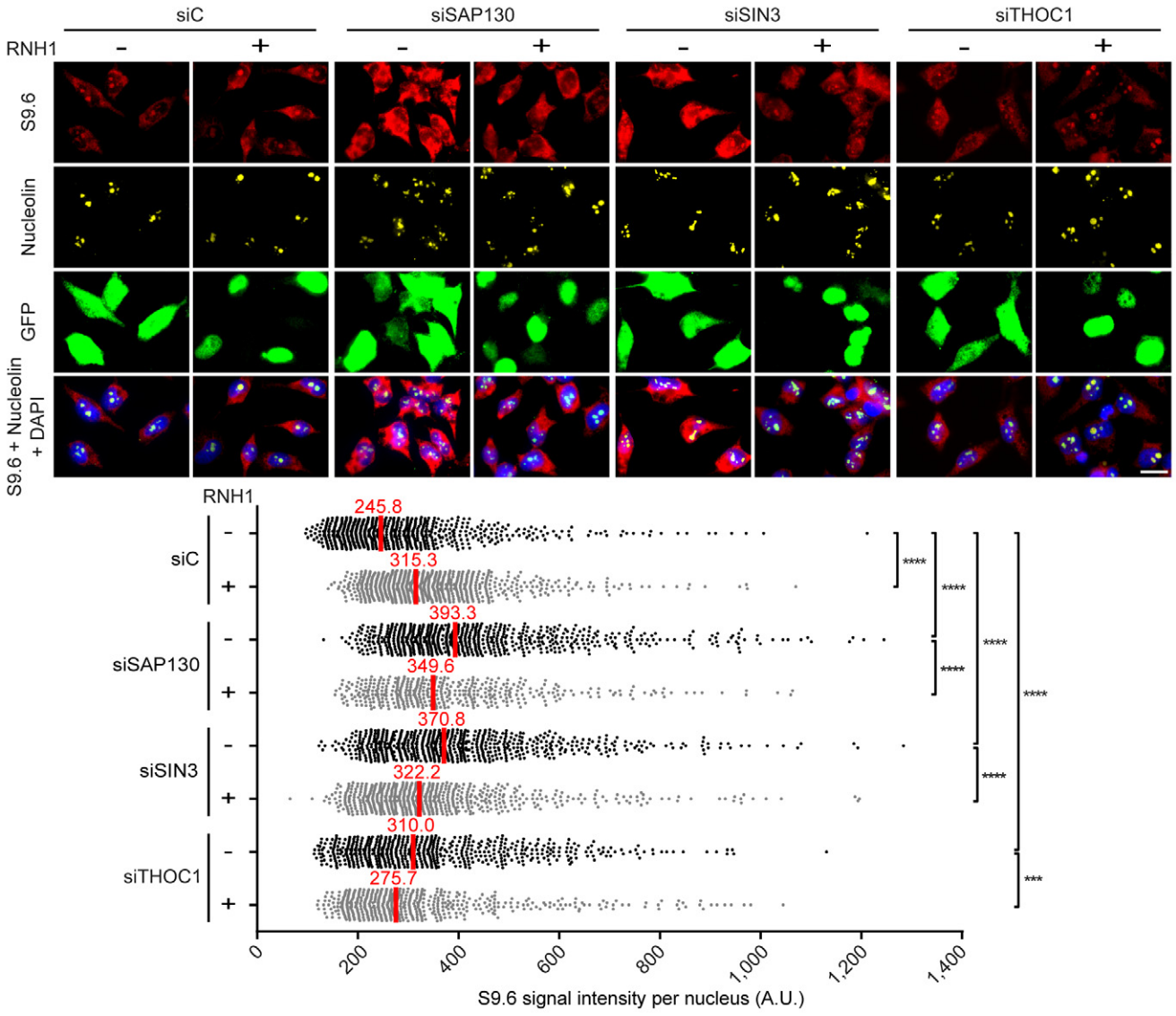

Figure 3. Nuclear RNA–DNA hybrid accumulation in Sin3A complex-depleted cells.

Immunostaining with S9.6 (red) and anti-nucleolin (yellow) antibodies in siC, siSAP130, siSIN3, and siTHOC1 HeLa cells transfected with pEGFP (−RNH1) or pEGFP-M27-H1 (+RNH1) for nuclear GFP-RNase H1 overexpression. More than 100 cells overexpressing GFP-RNase H1 (positive—green stained) or more than 100 cells transfected with the pEGFP vector (positive—green stained) were counted in each of the three experiments. The median of the S9.6 signal intensity per nucleus after nucleolar signal removal is shown ($n = 3$). Scale bar, 20 μm. ****$P < 0.0001$; ***$P < 0.001$ (Mann–Whitney U-test, two-tailed).

Higher levels of histone acetylation facilitate R-loop accumulation

Given that Sin3A regulates transcription through deacetylation of nucleosomes by histone deacetylases (HDACs) and recruitment of chromatin remodelers (Grzenda *et al*, 2009), and that Sin3A and THO depletions lead to a similar R-loop-dependent genome instability phenotype (Figs 2–5) and histone hyper-acetylation (Fig 6), our results suggest that histones possibly need to be deacetylated after transcription to prevent R-loop formation. Consequently, we used trichostatin A (TSA) an HDAC inhibitor (Yoshida *et al*, 1990) to determine whether high levels of acetylated histones facilitate R-loop accumulation. Importantly, treating untransfected HeLa cells with 250 nM TSA for 3 h significantly increased both histone H3 acetylation, as determined by Western blot, and RNA–DNA hybrid levels, as determined by IF (Fig 7A). The same results were obtained with suberoylanilide hydroxamic acid (SAHA), another HDAC inhibitor (Smith *et al*, 2010), as shown in Fig 7B, confirming that the effect is specifically due to HDAC inhibition. To confirm R-loop accumulation at the molecular level, we performed DRIP-qPCR in TSA-treated cells. The results confirm that histone deacetylation inhibition increases R-loops in the genes analyzed (Figs 7C and EV5A). These findings indicate that histone acetylation favors R-loop accumulation and that this is not due to a higher transcriptional activity, as assayed by RT–qPCR and RNAPII ChIP at different genes after TSA treatment (Fig EV5B).

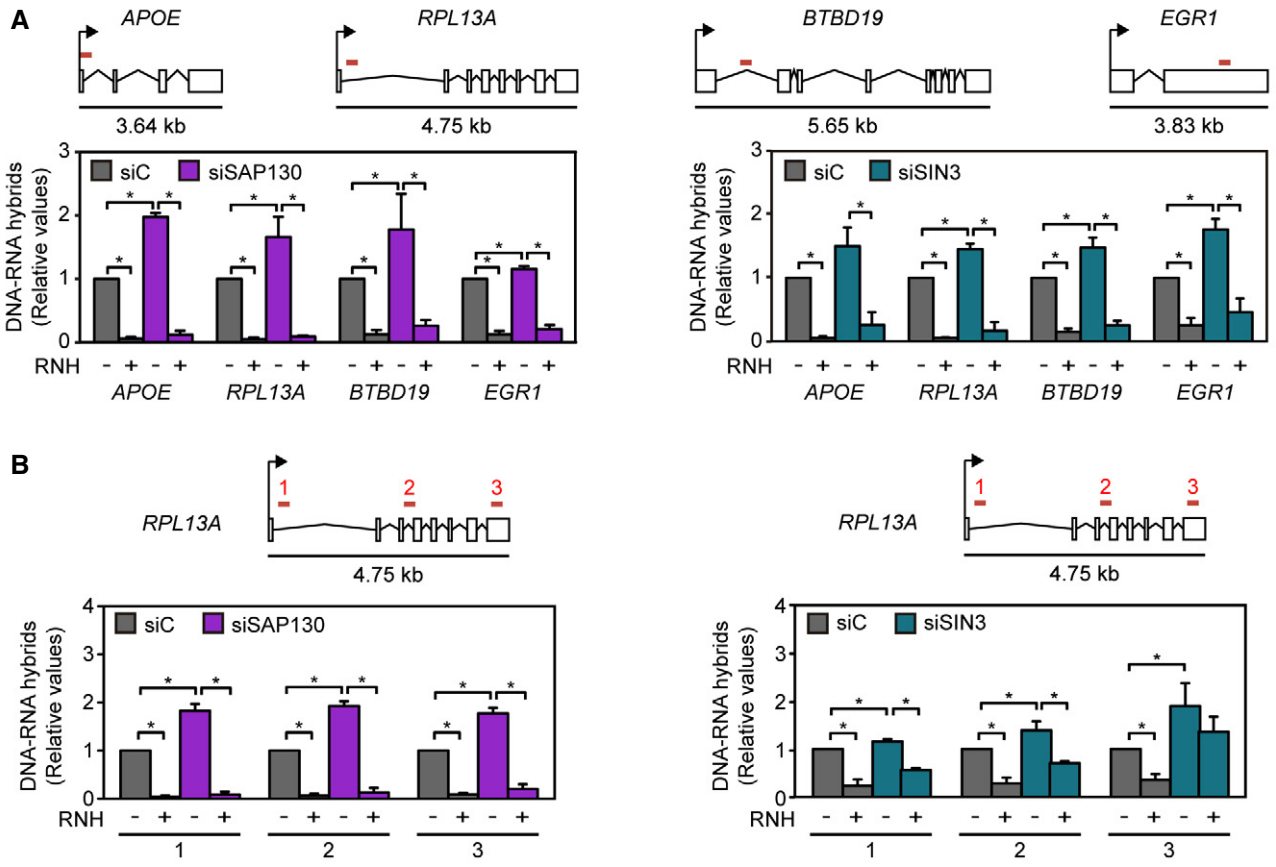

Figure 4. Sin3A complex-depletion increases R-loop accumulation at genes.

A DRIP-qPCR using the anti-RNA–DNA hybrids S9.6 monoclonal antibody in siC-, siSAP130-, and siSIN3-transfected HeLa cells at *APOE*, *RPL13A*, *BTBD19*, and *EGR1* genes.

B DRIP-qPCR in siC-, siSAP130-, and siSIN3-transfected HeLa cells at different regions of *RPL13A* gene.

Data information: (A, B) Schematic diagrams of genes are depicted. Red lines indicate the regions where PCR analyses were performed. Signal values normalized with respect to the siC control are plotted ($n = 3$) as mean ± SEM. *$P < 0.05$ (Mann–Whitney *U*-test). Absolute values of R-loop signals are provided in Fig EV3C and D.

Inhibition of histone acetylation suppresses genome instability in THOC1-depleted cells

The next question was whether or not histone deacetylation contributes to the mechanism by which THO prevents R-loop formation. If so, we should be able to suppress THO depletion phenotypes by maintaining histones hypo-acetylated in THOC1 knock-down cells. As expected, the histone acetyltransferase (HAT) inhibitor anacardic acid (AA) (Balasubramanyam *et al*, 2003) reduced histone acetylation in THOC1-depleted cells as shown by Western blot (Fig EV5C and D). Strikingly, anacardic acid also suppressed the increase in γH2AX foci, DNA breaks, and R-loops caused by THOC1 RNAi, as determined by IF, single-cell electrophoresis, and DRIP analysis, respectively (Figs 8A–C and EV5E). This treatment did not cause a reduction in transcription, as determined by RT–qPCR and RNAPII ChIP (Fig EV5F). Therefore, histone hypo-acetylation helps prevent R-loops and R-loop-mediated genome instability caused by THO depletion.

Replication fork stalling caused by SIN3- and THOC1-depleted cells

Since transcription-associated genome instability is mainly caused by replication fork (RF) stalling or collapse, which is increased by R-loops (Wellinger *et al*, 2006; Tuduri *et al*, 2009), we finally wondered whether this was also the case in THOC1 and SIN3 knock-down cells. Single-molecule DNA combing assays, used to analyze replication fork progression, showed that replication forks were on average faster in SIN3 knock-down than in control RNAi cells, as well as in THOC1 knock-down cells (Fig 9A), consistent with previously published results (Dominguez-Sanchez *et al*, 2011). Importantly, such fast velocity was accompanied by an increase in the frequency of replication fork stalling in these cells (Fig 9A), as determined by replication fork asymmetry (Tuduri *et al*, 2009). R-loops are mainly responsible for these phenotypes, since the increase in replication fork velocity and asymmetry is suppressed by RNaseH1 overexpression (Fig 9A). These results indicate that hyper-acetylated chromatin facilitates faster replication fork progression and that replication fork stalling can be a major determinant of R-loop-mediated genome instability.

Altogether, our results reveal a scenario in which an RNA-binding factor, THO, with a role in transcription elongation, RNA processing, and export, communicates with histone modifications to connect mRNP biogenesis with chromatin for protecting genome integrity. We propose a model in which

Published online: October 26, 2017
The EMBO Journal

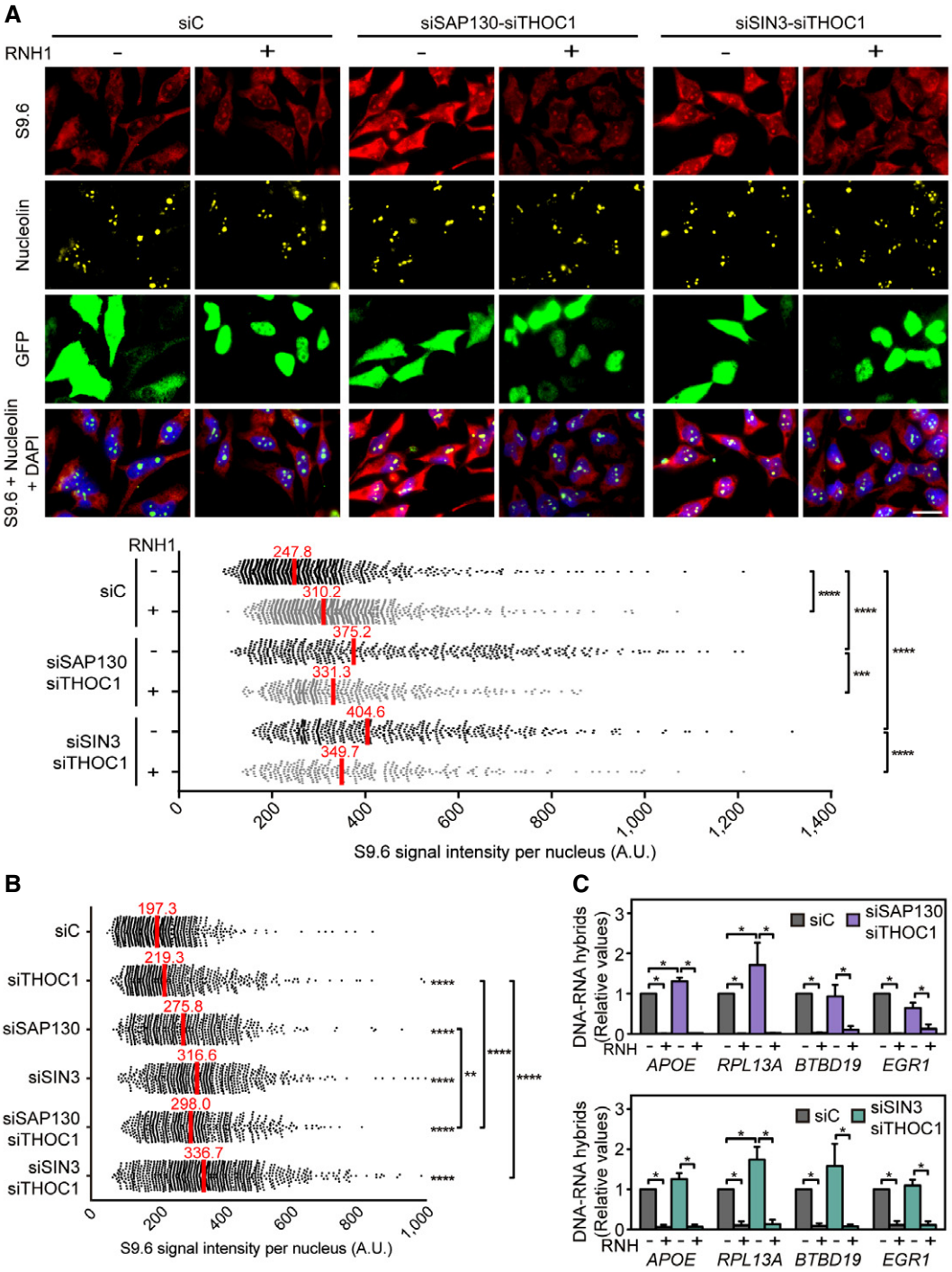

Figure 5. Nuclear RNA–DNA hybrid accumulation in THOC1-Sin3A complex-depleted cells.

A Immunostaining with S9.6 (red) and anti-nucleolin (yellow) antibodies in siC, siSAP130-siTHOC1, and siSIN3-siTHOC1 HeLa cells transfected with pEGFP (−RNH1) or pEGFP-M27-H1 (+RNH1) for nuclear GFP-RNase H1 overexpression. The median of the S9.6 signal intensity per nucleus after nucleolar signal removal is shown (n = 4). Scale bar, 20 μm. Other details as in Fig 3. Scale bar, 20 μm. Western blot of double siRNA depletions are shown in Fig EV1B.

B Quantification of S9.6 immmunofluorescence signal in siC, siSAP130-siTHOC1, and siSIN3-siTHOC1 HeLa cells transfected with pEGFP (−RNH1) or pEGFP-M27-H1 (+RNH1) for nuclear GFP-RNase H1 overexpression. Immunofluorescence images are shown in Fig EV4A. The median of the S9.6 signal intensity per nucleus after nucleolar signal removal is shown (n = 3). Other details as in Fig 3.

C DRIP-qPCR using the anti-RNA–DNA hybrids S9.6 monoclonal antibody in siC-, siSAP130-siTHOC1-, or siSIN3-siTHOC1-transfected HeLa cells at *APOE*, *RPL13A*, *BTBD19*, and *EGR1* genes. Signal values normalized with respect to the siC control are plotted (n = 4) as mean ± SEM. Absolute values of R-loop signals are provided in Fig EV4B.

Data information: For S9.6 signal quantification (A and B), more than 100 cells were scored in each experiment; ****$P < 0.0001$; ***$P < 0.001$; **$P < 0.01$ (Mann–Whitney U-test, two-tailed). DRIP assays (C) *$P < 0.05$ (Mann–Whitney U-test).

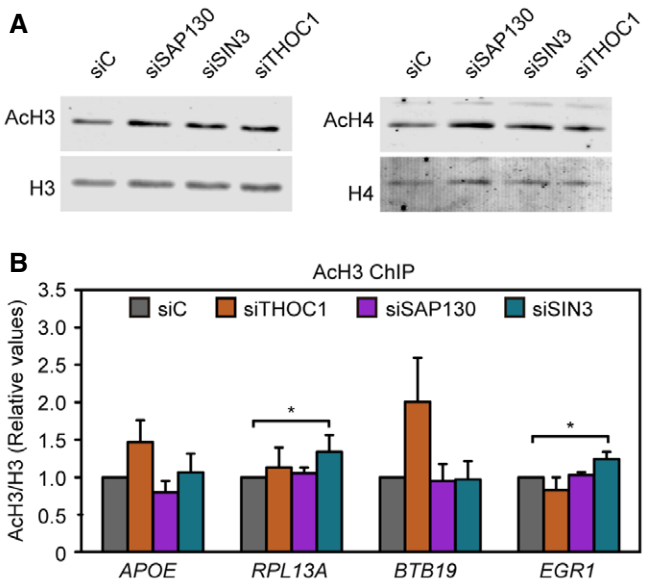

C

	HDAC activity (AFU/10^4 cells)
siC	107.9 ± 7.3
siTHOC1	82.0 ± 5.6
siSIN3	90.0 ± 6.2
siTHOC1-siSIN3	79.7 ± 5.7

Figure 6. Increased histone acetylation levels in siTHOC1 cells.

A Analysis of global histone H3 and histone H4 acetylation in siTHOC1-, siSAP130-, and siSIN3-transfected HeLa cells. Western blot was performed with antibodies raised against different acetylated residues. See Materials and Methods.

B ChIP analysis of AcH3 at *APOE*, *RPL13A*, *BTBD19*, and *EGR1* genes in siRNA-transfected HeLa cells. Values represent the ratios of precipitated DNA (IP) to input DNA (INPUT) normalized with respect to the siC control. Data are plotted as mean ± SEM (n = 3). *P < 0.05 (Mann–Whitney U-test). A significant difference was observed in siSIN3A cells at *RPL13A* and *ERG1* loci (P = 0.05); a difference not statistically significant was found in siTHOC1 cells at *APOE* and *EGR1* loci (P = 0.35), and no difference could be seen in the others.

C Histone deacetylase activity assay in siC-, siSIN3-, siTHOC1-, and siSIN3-siTHOC1-transfected HeLa cells. Total deacetylase activity was determined by fluorescence signal of deacetylated substrate (AFU=arbitrary fluorescence unit) and normalized with respect to the amount of cells. Data are plotted as mean ± SEM (n = 3).

Source data are available online for this figure.

THO depletion, as well as Sin3A depletion, leads to hyper-acetylated open chromatin that in turn facilitates co-transcriptional R-loops (Fig 9B). These structures would be an obstacle for the progression of the DNA polymerase that would cause replication problems leading to genome instability. Therefore, THO would suppress R-loops not only by ensuring an optimal mRNP structure that prevents the nascent RNA from hybridizing with the template (Huertas & Aguilera, 2003), but by directing histone deacetylation via Sin3A to transiently close chromatin.

Discussion

We have shown that human THOC1, a subunit of the THO/TREX complex, interacts with the Sin3A histone deacetylase complex. Depletion of the Sin3A complex leads to R-loop-mediated genome instability, similar to that conferred by THO mutants (Huertas & Aguilera, 2003). Consistently, inhibition of histone deacetylation results in R-loop accumulation as determined by DRIP assays and S9.6 immunofluorescence in cells depleted of the Sin3A complex, and in control cells after TSA and SAHA treatments. On the other hand, histone deacetylation activity is reduced in siTHOC1 cells, and, importantly, histone acetylation inhibition by anacardic acid suppresses DNA breaks and R-loops in THOC1-depleted cells. Therefore, the ability of the THO complex to prevent R-loops does not seem to be due only to its role in mRNP assembly alone (Aguilera, 2005), but also to its capacity to physically interact with the Sin3A complex. Strikingly, replication speed is faster in Sin3A- and THOC1-depleted cell lines, consistent with a more open chromatin conferred by high levels of histone acetylation that facilitates fork progression. Instead, replication forks stall more frequently, consistent with the model that R-loop-mediated genome instability could be caused by replication fork collapse. We propose that THO promotes transient histone deacetylation after transcription to prevent the RNA to hybridize back with the DNA template.

The Sin3A co-repressor complex regulates a wide variety of genes through its histone deacetylase activity and its interaction with a large number of DNA-transcription factors (Silverstein & Ekwall, 2005), and yeast *sin3*Δ mutants, selected in a global screen for mutants leading to chromosome instability, have been shown to prevent R-loop formation (Wahba *et al*, 2011). The interaction between THO and a transcriptional regulatory factor such as the Sin3A complex (Fig 1) supposes a new twist to our understanding of the mode of action of THO in R-loop prevention. R-loops accumulate in cells depleted of the Sin3A complex and cause DNA damage, transcription-associated genome instability, and replication, as shown by the fact that such phenotypes are suppressed by RNase H overexpression (Figs 2–4 and 9). Importantly, R-loop accumulation after histone deacetylation inhibition is not a direct consequence of an increase in transcription (Figs EV3 and EV5). Indeed, although transcription may enhance R-loop formation, R-loops may constitute a roadblock for the elongating RNA polymerase thus causing a reduction in transcription levels (Drolet *et al*, 1995; Huertas & Aguilera, 2003). Given the similar R-loop-dependent genome instability phenotype observed upon depletion of THO and Sin3A (Figs 2–5 and 9; Dominguez-Sanchez *et al*, 2011), our data suggest that these complexes talk to each other to reset chromatin after the passage of the RNAPII and thus prevent R-loop formation. Indeed, although R-loops accumulate in Sin3A-depleted cells at promoter-proximal regions of the genes analyzed (Fig 4A), consistent with the predominant binding of Sin3A around TSS (Sanz *et al*, 2016), they are also detected inside the gene body (Fig 4B). Along this same line, although Sin3A represses transcription at promoters, accumulating evidence indicates that Sin3A also localizes inside actively transcribed genes (Pile & Wassarman, 2000; Jelinic *et al*, 2011; Kadamb *et al*, 2013).

The detection of increased levels of histone acetylation and the reduced levels of histone deacetylase activity after THOC1 and SIN3 depletions suggest that a more open chromatin facilitates R-loop formation and that this may be a major reason as to why

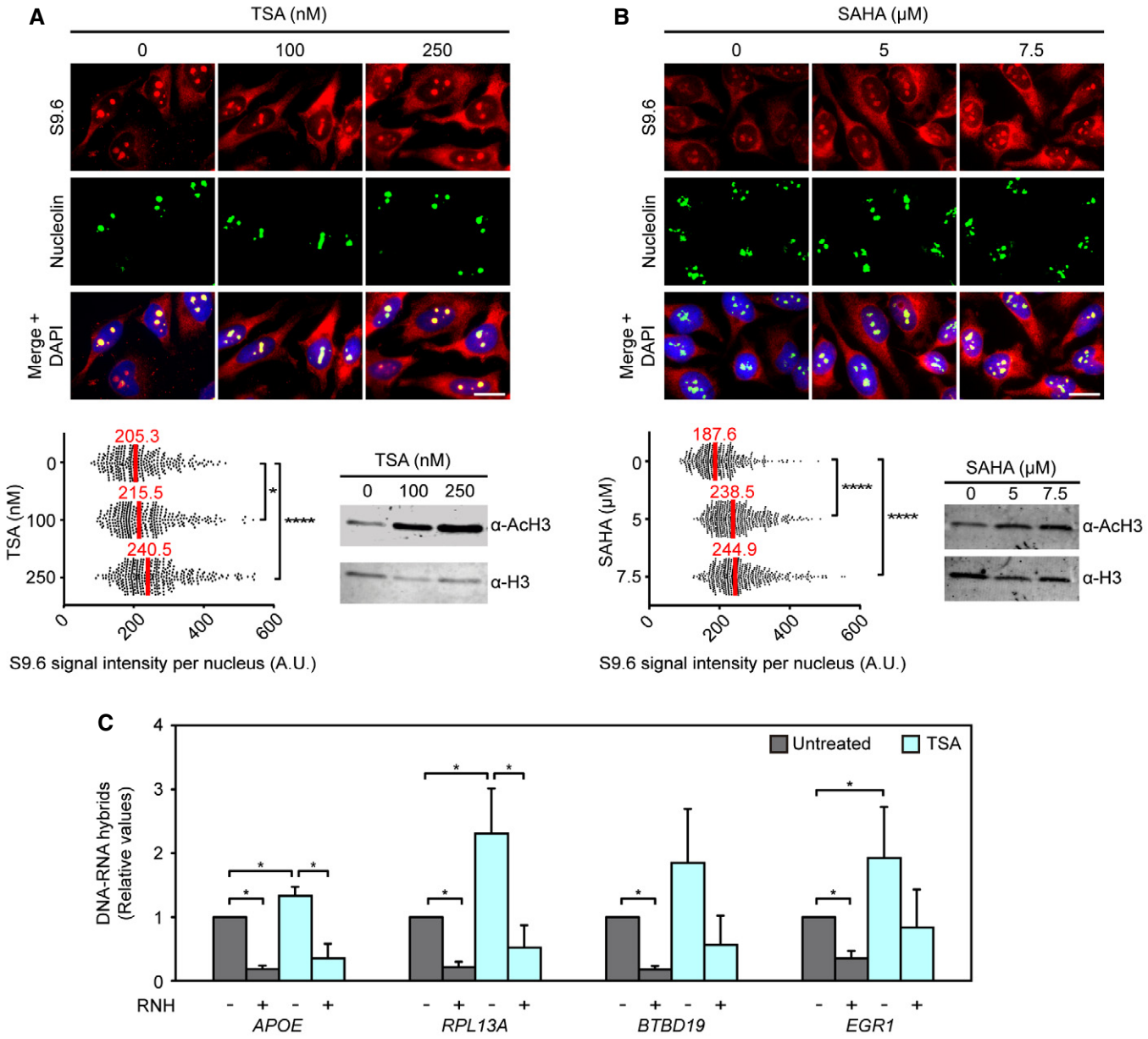

Figure 7. Inhibition of histone deacetylation increases R-loops.

A S9.6 immunofluorescence in HeLa cells untreated or treated for 3 h with 100 or 250 nM trichostatin A (TSA). Western blot analysis of histone H3 acetylation in cells untreated or treated is shown.

B S9.6 immunofluorescence in HeLa cells untreated or treated for 3 h with 5, or 7.5 μM SAHA. Western blot analysis of histone H3 acetylation in cells untreated or treated is shown.

C DRIP-qPCR using the S9.6 anti-RNA–DNA hybrid monoclonal antibody in cells untreated or treated with TSA. Signal values normalized with respect to the siC control are plotted (n = 3) as mean ± SEM. *P < 0.05 (Mann–Whitney U-test). Absolute values of R-loop signals are provided in Fig EV5A.

Data information: (A, B) The median of the S9.6 signal intensity per nucleus after nucleolar signal removal is shown (n = 3). *P < 0.05; ****P < 0.0001 (Mann–Whitney U-test, two-tailed). Scale bar, 20 μm.
Source data are available online for this figure.

THO-depleted cells accumulate R-loops (Fig 6). This hypothesis is supported by the striking result that the HAT inhibitor anacardic acid suppresses R-loops and genome instability in THO-depleted cells (Fig 8). Interestingly, recent genomewide analyses of chromatin modifications have revealed that active transcription and hyper-accessible chromatin are characteristics of R-loop hotspot DNA regions in normal cells (Sanz *et al*, 2016), which supports our model that a more open acetylated chromatin is more R-loop prone. At the same time, a more open chromatin state caused by hyper-acetylation explains a faster replication fork progression observed in both THO- and Sin3A-depleted cell lines. Importantly, despite their faster replication forks, both siTHO and siSin3A cells undergo high

Published online: October 26, 2017

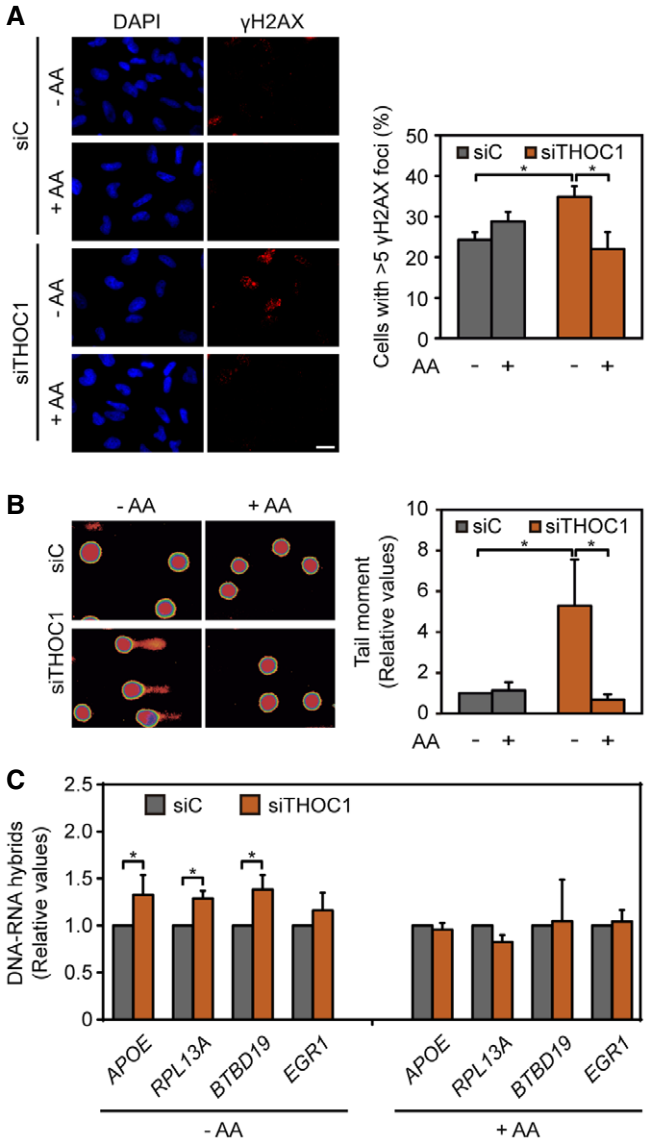

Figure 8. Histone deacetylation prevents R-loop and genome instability.

A Immunofluorescence of γH2AX in siC- and siTHOC1-depleted HeLa cells untreated or treated for 4 h with 30 μM anacardic acid (AA). Percentage of cells containing > 5 γH2AX foci (n = 4) is shown. Data are plotted as mean ± SEM. Scale bar, 20 μm.

B Single-cell electrophoresis of siTHOC1-depleted cells untreated or treated with AA. Mean ± SEM are plotted (n = 3).

C DRIP-qPCR analysis in siC- and siTHOC1-transfected cells untreated or treated with AA. Signal values normalized with respect to the respective siC controls are plotted as mean ± SEM (n = 3). Absolute values of R-loop signals are provided in Fig EV5E.

Data information: *P < 0.05 as determined by Student's t-test (A) or Mann–Whitney U-test (B, C).

frequency of replication fork stalling, consistent with this being the main cause of R-loop-mediated genome instability (Garcia-Muse & Aguilera, 2016), as demonstrated by the suppression of these phenotypes via RNase H1 overexpression (Fig 9A). These results are in agreement with previous data showing a genomewide role of THO complex preventing R-loop-dependent replication obstacles, as determined by an increase in recruitment of the Rrm3 helicase to active genes in yeast THO mutants (Gomez-Gonzalez *et al*, 2011). Interestingly, other mRNP factors such as SRSF1 have also been shown to prevent R-loop formation and replication fork collapses (Li & Manley, 2005; Tuduri *et al*, 2009). SRSF1 depletion increases fork asymmetry and also reduced fork velocity (Tuduri *et al*, 2009), which suggest that these two mRNP factors, SRSF1 and THO, are necessary for mRNP formation but prevent R-loops by different means. The faster fork velocity of siTHOC1 cells and siSIN3 can be the result of a more acetylated chromatin, whereas this may not be the case in SRSF1-depleted cells.

THO is not required for Sin3A recruitment to chromatin (Fig EV4D), but it could control histone deacetylation either directly or indirectly by influencing Sin3A activity (Fig 6C), stability, or modification to ensure transient chromatin closing after transcription (Fig 9B). The R-loop accumulation after double depletion of the THO and Sin3A complexes (Fig 5) supports a model in which a tight connection between RNA biogenesis and chromatin modification is necessary for the maintenance of genome integrity. Understanding this co-transcriptional chromatin dynamics *in vivo* requires new approaches to be developed in the future. The observation that R-loop-mediated transcription–replication collisions and genome instability are increased in yeast and human cells deficient in the FACT chromatin-reorganizing complex (Herrera-Moyano *et al*, 2014) supports the view that chromatin plays a crucial role in preventing R-loop-mediated genome instability. It is also possible that other epigenetic modifications linked to transcription that cause nucleosome depletion, such as histone methylation mediated by SETD2 (Carvalho *et al*, 2013), had an impact on transcription-associated genomic instability. Further work will be needed to decipher whether specific histone modifications, or whether acetylation of the THOC1 protein itself or some other subunit of the THO complex (Choudhary *et al*, 2009), are involved in preventing R-loop accumulation. However, the fast velocity of replication observed in siTHOC1 and siSIN3 cells supports the idea that histone deacetylation impairment is an important consequence of THOC1 depletion.

The physical and functional interaction between THO and Sin3A to prevent R-loops, R-loop-mediated genome instability, and replication fork stalling provides evidence for a functional crosstalk between RNA biogenesis and chromatin remodeling. This could be part of an mRNP surveillance mechanism to sense proper mRNP assembly and prevent harmful DNA structures, such as R-loops, by closing chromatin. In this sense, it is worth noting that specific epigenetic chromatin marks have been associated with harmful R-loops in the absence of THO in yeast, *Caenorhabditis elegans* and human cells (Castellano-Pozo *et al*, 2013), a conclusion supported by the finding of heterochromatin marks associated with R-loops in human fragile sites (Groh *et al*, 2014) and transcription termination regions (Skourti-Stathaki *et al*, 2014). We have proposed that these marks of chromatin compaction would explain why R-loop stalls replication forks and cause genome instability (Castellano-Pozo *et al*, 2013; Santos-Pereira & Aguilera, 2015). However, such chromatin modifications would certainly have to occur at later steps, once the R-loop has been formed and stabilized. Our recent identification of specific histone mutations in yeast able to induce high levels of R-loops that do not cause genome instability unless the ssDNA displaced in the R-loop is subjected to the action of the

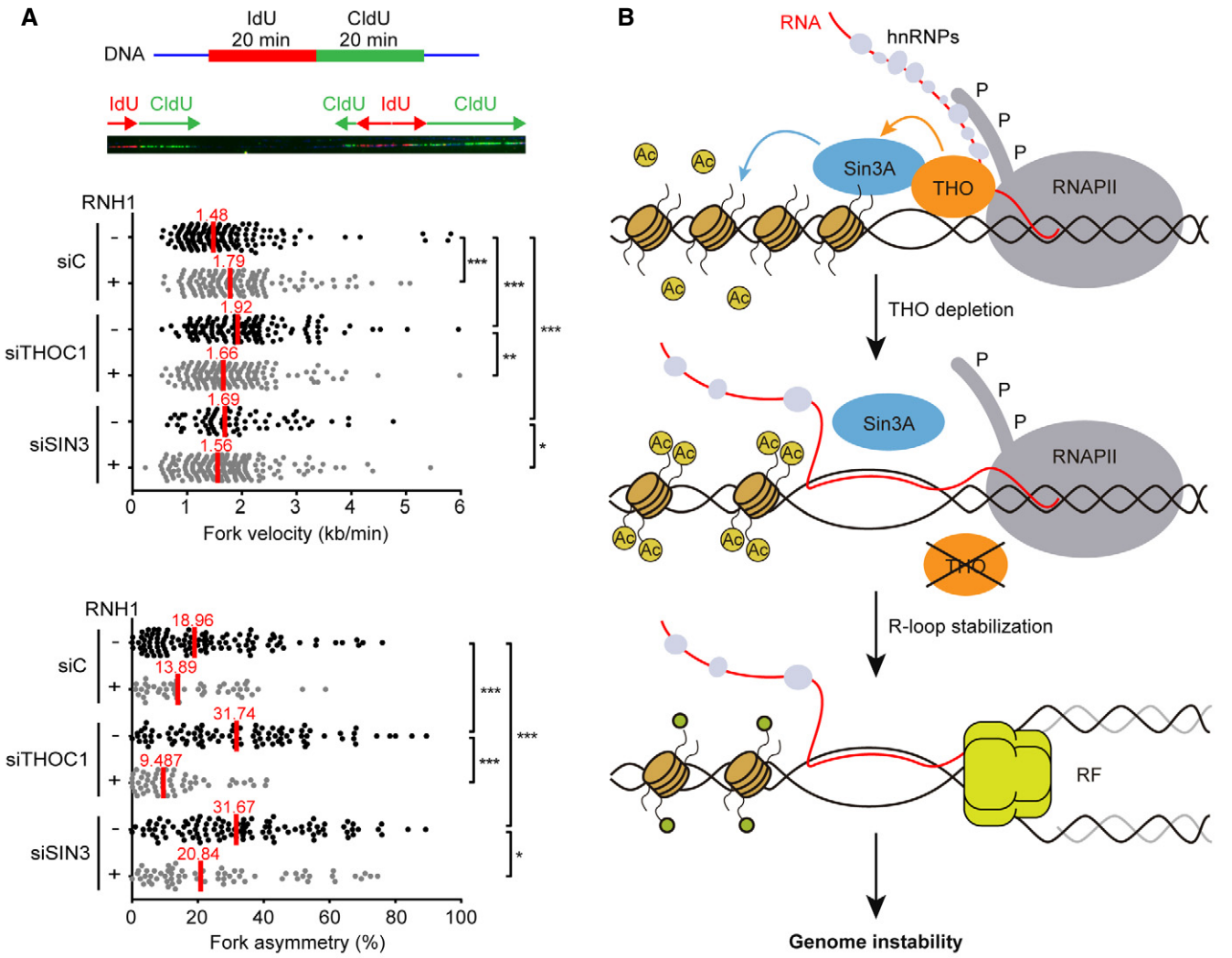

Figure 9. SIN3 and THOC1 depletions cause replication fork progression impairment.

A Effect of SIN3 and THOC1 depletion on DNA replication. Diagram and representative picture of DNA fibers labeled by IdU and CldU for single DNA molecule analysis in HeLa cells. Profiles of replication fork velocity and asymmetry of siC, siTHOC1, and siSIN3 HeLa cells transfected with pcDNA3 (−RNH1) or pcDNA3-RNaseH1 (+RNH1) for RNase H1 overexpression are shown. The data of three independent experiments were pooled together. *$P < 0.05$; **$P < 0.01$; ***$P < 0.001$ (Mann–Whitney *U*-test, two-tailed).

B Model to explain the functional relationship between THO and Sin3A complexes in the prevention of R-loop formation. During transcription, deacetylation of histones mediated by the Sin3A complex and majorly formation of an optimal mRNP particle mediated by THO help prevent R-loop formation. Depletion of THO would lead to the formation of a suboptimal mRNP, and a lower co-transcriptional action of Sin3A and hyper-acetylated chromatin, thus contributing to R-loop accumulation. A second step of R-loop stabilization would then contribute to genome instability and DNA replication impairment as recently proposed (Garcia-Pichardo *et al*, 2017). hnRNP: heterogenous ribonucleoproteins; RF: replication fork.

human AID cytidine deaminase (Garcia-Pichardo *et al*, 2017) strongly supports this notion. Such a phenomenon would certainly be different to the early chromatin modifications described here as an early step to favor R-loop formation.

In summary, our observation that the THO mRNP biogenesis factor interacts physically and functionally with the Sin3A deacetylase complex provides strong evidence of a functional crosstalk between nascent RNA binding proteins and chromatin modifiers that is crucial for maintenance of genome integrity. Given the deregulation of THOC1 and Sin3A in cancer cells, it would be important to further investigate this relationship and whether or not additional proteins are required for this crosstalk.

Materials and Methods

Human cells culture, transfection reagents, and plasmids

HeLa and HEK293T cells were bought from ECACC (European Collection of Cell Cultures) and ATCC (American Type Culture Collection). HeLa and HEK293T cells were cultured in Dulbecco's modified Eagle's medium (DMEM; GIBCO, Thermo Scientific, Waltham, MA) supplemented with 10% heat-inactivated fetal bovine serum at 37°C (5% CO_2).

ON-TARGET SMARTpool of siRNA from Dharmacon were used for all depletions. Independent siRNAs from siSAP130 and siSIN3

pools were also used. Transient transfection of siRNA was performed using DharmaFECT 1 (Dharmacon) according to the manufacturer's instructions. Fugene (Promega, Madison, WI, USA) or Lipofectamine 2000 or Lipofectamine 3000 (Invitrogen, Carlsbad, CA) was used for plasmid transfection. Assays were performed 48 or 72 h after siRNA transfection.

Plasmids used were the following: pcDNA3 (Invitrogen); pcDNA3-RNaseH1, containing the full-length RNase H1 cloned into pcDNA3 (ten Asbroek *et al*, 2002). pEGFP (−RNH1) or pEGFP-M27-H1 (+RNH1) for GFP-RNase H1 overexpression (Cerritelli *et al*, 2003).

Antibodies

The following antibodies were used: anti-SAP130 (ab114978; Abcam), anti-SAP130 (ab111739), anti-THOC1 (ab487; Abcam), anti-mSin3A (ab3479; Abcam), S9.6 antibody (hybridoma cell line HB-8730), anti-nucleolin (ab50279; Abcam), anti-γH2AX (clone JBW301; Upstate), anti-beta-actin (ab8227; Abcam), anti-acetyl-histone H3 (ab47915; Abcam), anti-acetyl-histone H3 (06-599 Merck), anti-histone H3 (ab1791; Abcam), anti-histone H3 (1B1B2) (14269 Cell Signaling), anti-acetyl-histone H4 (AcH4) (06-598; Millipore), anti-histone H4 (ab7311; Abcam), anti-histone H3 (acetyl K14) antibody (ab52946; Abcam), anti-Pol II (H-224) (sc-9001; Santa Cruz Biotechnology), and anti-GFP (ab5450).

Reagents

Cordycepin (C3394; Sigma), 5,6-dichlorobenzimidazole 1-β-D-ribofuranoside (DRB) (D1916; Sigma), trichostatin A (TSA) (T8552; Sigma), suberoylanilide hydroxamic acid (SAHA) (SML0061; Sigma), anacardic acid (AA) (172050; Millipore), and dimethyl sulfoxide (DMSO) (D4540; Sigma) reagents were used.

Yeast two-hybrid assay

Yeast two-hybrid screening was performed with the Matchmaker Gold Yeast Two-Hybrid System (Clontech 630489), using THOC1 protein as a bait and the Mate&Plate Library Universal Human (normalized) (Clontech 630480) to produce prey proteins. cDNA library is cloned into a GAL4 activation domain vector (pGADT7) and transformed into yeast strain Y187. THOC1 cDNA (from IMAGE clone 4046908, LifeSciences) was cloned into pGBKT7 vector fused to the Gal4 DNA-binding domain (pGALBD-THOC1). Primers used for cloning were as follows: BD-THOC1_FW (5′-CATATGGC CATGG AGGCCGAATTCATGTCTCCGACGCCGCCGCTCTTC-3′) and BD-THOC1_RV (5′-GCAGGTCGACGGATCCCTAACTATTTGTCTCATTG TCATT-3′). Yeast strain Y2HGold transformed with vector pGALBD-THOC1 was mated with the strain Y187 transformed with the cDNA library and grown at 30°C for 20 h to obtain zygotes. The culture was plated onto selective medium (SC-Trp-Leu+(X-α-Gal)+Aureobasidin (AbA) and incubated at 30°C for 3–5 days. Blue colonies were streaked onto high stringency medium (SC-Ade-His-Trp-Leu+(X-α-Gal)+AbA) and incubated at 30°C for 3–5 days. Prey plasmids from the blue colonies selected on high stringency plates were rescued, and inserts were sequenced. Standard procedures were used to grow and maintain yeast strains.

Cell proliferation

For proliferation assays, HeLa cells were plated in one well of a six-well plate and were transfected with siRNA at 30–50% confluence the following day. 48 h after transfection, cells were plated in wells of 96-well plates (2,000 cells/well). The first quantification, which was considered the day 0, was performed after 7 h. Cells were transfected again 3 days after first transfection with 2/5 of siRNA standard amount. Cell number quantification was performed using the Cell Proliferation reagent WST-1 (4-[3-84-Iodophenyl)-2-(4-nitrophenyl)2H-5-tetrazolio]-1,3-benzene disulfonate) (Roche) following the manufacturer's protocol. Absorbance was measured using microplate (ELISA) reader VARIOSKAN FLASH (Thermo) at 450 nm with a reference wavelength of 690 nm. Absorbance values were normalized to the value at the day 0 and represented as arbitrary units (A.U.). Measurements were performed each 24 h.

Cell cycle analysis

Synchronization of cells population in G1/S to monitored S-phase progression was performed using a double thymidine block. HeLa cells were transfected with siRNA at 30–40% confluence. 24 h after transfection, growth medium was replaced with fresh medium containing 2 mM thymidine and cells were incubated for 19 h under normal conditions. After three washes in PBS, cells were released in fresh complete medium and incubated under normal conditions for 7 h. Following incubation, medium was replaced with fresh medium containing 2 mM thymidine and cells were incubated for 17–19 h under normal conditions. Finally, cells were washed three times in PBS and released in fresh complete medium. 20 min before collect the samples, cells were incubated with EdU (20 μM) to allow EdU incorporation in replicating cells. Time points were collected 0, 1, 2, 4, 6, and 9 h after release. EdU incorporation was detected using Click-iT assay kit (Thermo Fisher Scientific) following the manufacturer's protocol. Three population of cells were analyzed based on their DNA content and EdU signal: G1 (with 1n DNA content and no EdU signal), S (with DNA content between 1n and 2n and EdU signal), and G2-phase (with 2n DNA content and no EdU incorporation) cells.

Apoptosis

Apoptotic cells were detected by flow cytometry according to published procedures by analysis of sub-G1 DNA content (Gong *et al*, 1994). Basically, cells were washed with phosphate-buffered saline (PBS), fixed in cold 70% ethanol, and then stained with propidium iodide while treating with RNase A. Quantitative analyses of sub-G1 cells were carried out in a FACScan cytometer using the Cell Quest software (BD Biosciences).

Analysis of RNA synthesis by ethynyl uridine incorporation

RNA synthesis was measured using the Click-It RNA Alexa 594 imaging kit (Cat. No. C10330; Life Technologies) according to the manufacturer's instructions. HeLa cells were seeded at a density of 8×10^5 in 60-mm dishes. Following 24 h after seeding, cells were treated with 50 μM of cordycepin or 100 μM of DRB in complete medium during 4 h. The untreated controls were

exposed to the same volume of the corresponding treatment vehicles (water and DMSO, respectively). During the last 30 min of drug exposure, cells were supplemented with ethynyl uridine (EU) at the final concentration of 1 mM. Subsequently, cells were fixed in 3.7% formaldehyde for 15 min, washed three times with PBS, permeabilized with 0.5% Triton X-100 for 15 min, washed again with PBS, and then incubated with Alexa Fluor 594-azide in Click-iT reaction cocktail for 30 min. Following one wash with the Click-iT rinse buffer and two washes with PBS, nuclei were counterstained with 10 μg/ml DAPI in PBS for 5 min, washed three more times, and mounted with ProLong Gold antifade reagent (Invitrogen). Random images were acquired with a 40× objective, and EU intensity was scored using the MetaMorph software.

Co-immunoprecipitation

For co-immunoprecipitation assays, HEK193T cells (5×10^6) were lysed for 30 min on ice in 200 μl of extraction buffer (10 mM Tris–HCl pH 7.5, 150 mM NaCl, 0.5 mM EDTA, 0.5% (vol/vol) NP-40, 1 mm PMSF, and protease inhibitor cocktail). Lysates were cleared by centrifugation for 15 min at 12,000 *g* at 4°C, and 1:10 of cell extract was used for the input loading control. The lysate was diluted by adding the same volume of dilution buffer (10 mM Tris–HCl pH 7.5, 150 mM NaCl, 0.5 mM EDTA, 1 mM PMSF, and protease inhibitor cocktail) and incubated for 2 h at 4°C with 50 μl of Dynabeads Protein A (Invitrogen) pre-equilibrated in PBS-0.5% BSA and conjugated with 5 μg of polyclonal specific antibody anti-SAP130 or anti-SIN3, or with 2.5 μg of anti-THOC1. The same amount of lysate was incubated with beads without antibody and was used as control. Beads were washed twice with phosphate-buffered saline (PBS) and three times with dilution buffer with 0.2% NP-40. Bound proteins were eluted by boiling the beads for 10 min in 25 μl of 2× Laemmli loading buffer and analyzed by Western blot with the following antibodies: anti-THOC1 (1:5,000), anti-SIN3 (1:1,000), and anti-SAP130 (1:2,000).

Proximity ligation assay

The proximity ligation assay was performed as described (Soderberg *et al*, 2006; Bhatia *et al*, 2014) with reagents from Duolink *In Situ* Red Starter Kit (Olink Biosciences) in accordance with the manufacturer's instructions. Cells were pre-permeabilized with cold 0.1% Triton in PBS on ice for 1 min and then were fixed in 2% formaldehyde in PBS for 20 min and permeabilized with 70% ethanol for 5 min at −20°C. PBS-3% BSA was used as blocking solution and for primary antibodies and PLA probes dilution. The following antibodies were used: anti-THOC1 (1:500 dilution), anti-SAP130 (1:50), and anti-SIN3 (1:50). For negative controls, everything was performed identically, except that only one of the primary antibodies was added.

γH2AX and S9.6 immunofluorescence

Analysis of DNA damage foci γH2AX immunofluorescence was performed as previously described (Dominguez-Sanchez *et al*, 2011). More than 100 cells were scored in each experiment. S9.6 (hybridoma cell line HB-8730) immunofluorescence was performed as previously described (Garcia-Rubio *et al*, 2015) using secondary antibodies conjugated with Alexa 488, Alexa 594, and Alexa 647. Images of IF were acquired with a Leica DM6000 microscope equipped with a DFC390 camera (Leica) at 63× magnification, and data acquisition was performed with LAS AF (Leica). S9.6 signal intensity and γH2AX foci measurements were analyzed and processed with the MetaMorph v7.5.1.0 (Molecular Probes) image analysis software. More than 100 cells were scored in each experiment.

Single-cell electrophoresis

Single-cell electrophoresis or comet assays were performed as described (Dominguez-Sanchez *et al*, 2011) using a commercial kit (Trevigen, Gaithersburg, MD, USA) following the manufacturer's protocol. For neutral comet assays, electrophoresis was performed at 35 V for 15 min at 4°C. Comet slides were stained with SYBR Green, and images were captured at 10× magnification. Comet tail moments were analyzed using Comet-score (version 1.5) or TriTek CometScore Professional (version 1.0.1.36) software. At least 100 cells were scored in each experiment to calculate the median of the tail moment.

DNA–RNA immunoprecipitation (DRIP)

DRIP assays were performed by immunoprecipitating DNA–RNA hybrids using the S9.6 antibody from gently extracted and enzymatically digested DNA, treated or not with RNase H *in vitro* as described (Herrera-Moyano *et al*, 2014; Garcia-Rubio *et al*, 2015). The relative abundance of DNA–RNA hybrid immunoprecipitated in each region was normalized to input values and to the siC control. In all analyses, a region of *SNRPN* gene was used as negative control because it shows low levels of R-loops, as previously reported (Bhatia *et al*, 2014; Herrera-Moyano *et al*, 2014; Garcia-Rubio *et al*, 2015). DRIP assays were performed 72 h after siRNA transfection. All experiments were performed in triplicate; mean and standard error of the mean (SEM) of results are provided.

mRNA quantification

cDNA synthesis and qPCR were performed as previously described (Dominguez-Sanchez *et al*, 2011). Relative mRNA expression values of the indicated genes were calculated by the $2^{-\Delta CT}$ method, using the expression of the *HPRT* housekeeping gene as endogenous control. Primers used in real-time qPCR are described below.

RNA primers for real-time qPCR

The following primers were used for real-time quantitative PCR (qPCR): APOE_1, 5′-GGGAGCCCTATAATTGGACAAGT-3′ (forward) and 5′-CCCGACTGCGCTTCTCA-3′ (reverse); APOE_3, 5′-AA GCTGGAGGAGCAGGCC-3′ (forward) and 5′-ACTGGCGCTGCATGT CTTC-3′ (reverse); RPL13A_1, 5′-GCTTCCAGCACAGGACAGGTAT-3′ (forward) and 5′-CAC CCACTACCCGAGTTCAAG-3′ (reverse); RPL13A_2, 5′-ACTGGGCAGGCCTCACACT-3′(forward) and 5′-CGCT TGCGGAGGAAAGC-3′(reverse); RPL13A_3, 5′-GGGAGCAAGGAAAG GGTCTTA-3′ (forward) and 5′-ACAATTCTCCGAGTGCTTTCAAG-3′ (reverse); BTBD19, 5′-CCCCAAAGGGTGGTGACTT-3′ (forward) and

5′-TTCACATTACCCAGACCAGACTGT-3′ (reverse); BTBD19_3, 5′-GCCCCGGGAGCATCAC-3′ (forward) and 5′-CCCGGCGTTGGAT CATT-3′ (reverse); EGR1, 5′-GCCAAGTCCTCCCTCTCTACTG-3′ (forward) and 5′-GGAAGTGGGCAGAAAGGATTG-3′ (reverse); SNRPN, 5′-TGCCAGGAAGCCAAATGAGT-3′ (forward) and 5′-TCCCTCTTGG CAACATCCA-3′ (reverse); HPRT, 5′-GGACTAATTATGGACAGGAC TG-3′ (forward) and 5′-TCCAGCAGGTCAGCAAAGAA-3′ (reverse).

Chromatin immunoprecipitation (ChIP)

HeLa cells were crosslinked and processed for ChIP as described (Hecht & Grunstein, 1999) with minor modifications. In brief, cells were crosslinked for 10 min with 1% formaldehyde, resuspended in 2.5 ml of cell lysis buffer (5 mM PIPES pH 8, 85 mM KCl, 0.5% NP-40, 1 mM PMSF, and protease inhibitor cocktail), then centrifuged, and 1 ml of nuclei lysis buffer (1% SDS, 10 mM EDTA, 50 mM Tris–HCl pH 8, 1 mM PMSF, and protease inhibitor cocktail) was added. Chromatin was sonicated on the maximum intensity setting, with fifteen pulses of 30 s on and 30 s off in Bioruptor (Diagenode), to obtain ~400-bp fragments. For each immunoprecipitation, 25 μg of chromatin was diluted up to 1,300 μl with IP buffer (0.01% SDS, 1.1% Triton X-100, 1.2 mM EDTA, 16.7 mM Tris–HCl pH 8, 167 mM NaCl). 100 and 1,200 μl of diluted chromatin were used for input and immunoprecipitation, respectively. Chromatin was incubated overnight at 4°C with 5 μg of antibody. A negative control without antibody was used to calculate the background signal. Chromatin-antibody complexes were immunoprecipitated for 2 h with 30 μl of Dynabeads Protein G (Invitrogen) at 4°C and washed once with wash buffer 1 (0.1% SDS, 1% Triton X-100, 2 mM EDTA, 20 mM Tris–HCl pH 8, 150 mM NaCl), once with wash buffer 2 (0.1% SDS, 1% Triton X-100, 2 mM EDTA, 20 mM Tris–HCl pH 8, 500 mM NaCl), once with wash buffer 3 (0.25 M LiCl, 1% NP-40, 1% sodium deoxycholate, 1 mM EDTA, 10 mM Tris–HCl pH 8), and twice with 1× TE. Input and immunoprecipitate were then un-crosslinked in TE-1% SDS and treated with proteinase K. DNA was isolated using NucleoSpin Gel and PCR Clean-up kit (Macherey-Nagel), and qPCR was performed with the primers listed above. Signal values in the different regions were calculated as the ratio between the DNA amount immunoprecipitated subtracting the background signal (IP) and the total amount of DNA (input) of each region.

HDAC activity assay

HDAC activity was measured with the HDAC fluorometric Cellular Activity Assay kit (Enzo) according to the manufacturer's instructions. HeLa cells were reverse-transfected with siRNA at the final concentration of 140 nM using Lipofectamine 3000 (Invitrogen). For each condition, cells were seeded and transfected in triplicate in a 96-well plate at the concentration of 6×10^4 cells/well. 72 h after transfection, cells were incubated with media containing 0.2 mM Fluor de Lys Substrate (BML-KI104) for 2 h at 37°C. Subsequently, developer solution and TSA trichostatin (TSA) at the final concentration of 2 μM were added to stop the deacetylation process. After addition of developer, plates were incubated for an additional 2 h at 37°C and fluorescence (Ex. 360 nm, Em. 460 nm) was measured using a VARIOSKAN FLASH (Thermo) microplate reader. In parallel, a duplicate of each sample was plated to calculate the number of cells in each condition. Cell number quantification was performed using the absorbance values of the Cell proliferation reagent WST-1 (see Materials and Methods—Cell proliferation) with the reference of a standard curve with known cell number. In each condition, HDAC activity was calculated as the fluorescence signal of deacetylated substrate, represented as fluorescence arbitrary units (AFU), normalized to the number of cells.

DNA combing

DNA combing was performed as previously described (Dominguez-Sanchez *et al*, 2011; Bianco *et al*, 2012). Cells were transfected with pcDNA3 or pcDNA3 RNaseH1 for 48 h. Iododeoxyuridine and chlorodeoxyuridine labels were added for 20 min each. DNA molecules were counterstained with an anti-ssDNA antibody (DSHB, 1:500) and an anti-mouse IgG coupled to Alexa 647 (A21241, Invitrogen, 1:50). CldU and IdU were detected with BU1/75 (AbCys, 1:20) and BD44 (Becton Dickinson, 1:20) anti-BrdU antibodies, respectively. Secondary antibodies used were goat anti-mouse IgG Alexa 546 (A21123, 1:50) and chicken anti-rat Alexa 488 (A21470, 1:50). DNA fibers were analyzed on a Leica DM4000 microscope equipped with a DFC365 FX camera (Leica). Data acquisition was performed with LAS AX (Leica). Representative images of DNA fibers were assembled from different microscopic fields of view and were processed as described. To measure fork replication velocity, cells were pulse-labeled with IdU and CIdU and the distance covered by individual forks during the pulse (kb/min) was determined as previously described (Dominguez-Sanchez *et al*, 2011). Replication asymmetry was calculated by dividing (longest green tract – shortest green tract) by the longest tract in divergent CIdU tracks.

Statistical analysis

For single-cell electrophoresis assays and DRIP, nonparametric Mann–Whitney *U*-test was used. For γH2AX foci analysis, paired Student's *t*-test (parametric) was used. For S9.6 immunofluorescence and DNA combing data analysis, Mann–Whitney *U*-test two-tailed was performed. In general, a *P*-value < 0.05 was considered as statistically significant (****$P < 0.0001$; ***$P < 0.001$; **$P < 0.01$; *$P < 0.05$). Data were analyzed with EXCEL (Microsoft) or GraphPad Prism software. The statistical test used in each experiment is mentioned in the figure legend.

Expanded View for this article is available online.

Acknowledgements

We thank C. Tous for technical assistance with two-hybrid analysis; J. C. Reyes and A. G. Rondón for comments on the manuscript, and D. Haun for style supervision, and R.J. Crouch for the gift of the plasmid pEGFP-M27-H1. Research was funded by the European Research Council (ERC2014 AdG669898 TARLOOP), the Spanish Ministry of Economy and Competitiveness (BFU2013-42918-P and BFU2016-75058-P), the Junta de Andalucía (BIO1238), and the European Union (FEDER). I.S.A. and C.P.C were recipients of FPU and FPI pre-doctoral training grants from the Spanish Ministries of Education, Culture and Sports and of Economy and Competitiveness, respectively.

Author contributions

IS-A, CP-C, AB-F, ET, and RL performed the experiments. ISA, RL, and AA designed the experiments. ISA, RL, and AA wrote the manuscript. All authors read, discussed, and agreed with the final version of the manuscript.

Conflict of interest

The authors declare that they have no conflict of interest.

References

Aguilera A (2005) mRNA processing and genomic instability. *Nat Struct Mol Biol* 12: 737 – 738

Andersen DS, Tapon N (2008) *Drosophila* MFAP1 is required for pre-mRNA processing and G2/M progression. *J Biol Chem* 283: 31256 – 31267

ten Asbroek AL, van Groenigen M, Nooij M, Baas F (2002) The involvement of human ribonucleases H1 and H2 in the variation of response of cells to antisense phosphorothioate oligonucleotides. *Eur J Biochem* 269: 583 – 592

Balasubramanyam K, Swaminathan V, Ranganathan A, Kundu TK (2003) Small molecule modulators of histone acetyltransferase p300. *J Biol Chem* 278: 19134 – 19140

Bhatia V, Barroso SI, Garcia-Rubio ML, Tumini E, Herrera-Moyano E, Aguilera A (2014) BRCA2 prevents R-loop accumulation and associates with TREX-2 mRNA export factor PCID2. *Nature* 511: 362 – 365

Bianco JN, Poli J, Saksouk J, Bacal J, Silva MJ, Yoshida K, Lin YL, Tourriere H, Lengronne A, Pasero P (2012) Analysis of DNA replication profiles in budding yeast and mammalian cells using DNA combing. *Methods* 57: 149 – 157

Carvalho S, Raposo AC, Martins FB, Grosso AR, Sridhara SC, Rino J, Carmo-Fonseca M, de Almeida SF (2013) Histone methyltransferase SETD2 coordinates FACT recruitment with nucleosome dynamics during transcription. *Nucleic Acids Res* 41: 2881 – 2893

Castellano-Pozo M, Santos-Pereira JM, Rondon AG, Barroso S, Andujar E, Perez-Alegre M, Garcia-Muse T, Aguilera A (2013) R loops are linked to histone H3 S10 phosphorylation and chromatin condensation. *Mol Cell* 52: 583 – 590

Cerritelli SM, Frolova EG, Feng C, Grinberg A, Love PE, Crouch RJ (2003) Failure to produce mitochondrial DNA results in embryonic lethality in Rnaseh1 null mice. *Mol Cell* 11: 807 – 815

Chavez S, Beilharz T, Rondon AG, Erdjument-Bromage H, Tempst P, Svejstrup JQ, Lithgow T, Aguilera A (2000) A protein complex containing Tho2, Hpr1, Mft1 and a novel protein, Thp2, connects transcription elongation with mitotic recombination in *Saccharomyces cerevisiae*. *EMBO J* 19: 5824 – 5834

Choudhary C, Kumar C, Gnad F, Nielsen ML, Rehman M, Walther TC, Olsen JV, Mann M (2009) Lysine acetylation targets protein complexes and co-regulates major cellular functions. *Science* 325: 834 – 840

Dominguez-Sanchez MS, Barroso S, Gomez-Gonzalez B, Luna R, Aguilera A (2011) Genome instability and transcription elongation impairment in human cells depleted of THO/TREX. *PLoS Genet* 7: e1002386

Drolet M, Phoenix P, Menzel R, Masse E, Liu LF, Crouch RJ (1995) Overexpression of RNase H partially complements the growth defect of an *Escherichia coli* delta topA mutant: R-loop formation is a major problem in the absence of DNA topoisomerase I. *Proc Natl Acad Sci USA* 92: 3526 – 3530

Fleischer TC, Yun UJ, Ayer DE (2003) Identification and characterization of three new components of the mSin3A corepressor complex. *Mol Cell Biol* 23: 3456 – 3467

Gan W, Guan Z, Liu J, Gui T, Shen K, Manley JL, Li X (2011) R-loop-mediated genomic instability is caused by impairment of replication fork progression. *Genes Dev* 25: 2041 – 2056

Garcia-Muse T, Aguilera A (2016) Transcription-replication conflicts: how they occur and how they are resolved. *Nat Rev Mol Cell Biol* 17: 553 – 563

Garcia-Pichardo D, Canas JC, Garcia-Rubio ML, Gomez-Gonzalez B, Rondon AG, Aguilera A (2017) Histone mutants separate R loop formation from genome instability induction. *Mol Cell* 66: 597 – 609.e595

Garcia-Rubio ML, Perez-Calero C, Barroso SI, Tumini E, Herrera-Moyano E, Rosado IV, Aguilera A (2015) The fanconi anemia pathway protects genome integrity from R-loops. *PLoS Genet* 11: e1005674

Ginno PA, Lim YW, Lott PL, Korf I, Chedin F (2013) GC skew at the 5′ and 3′ ends of human genes links R-loop formation to epigenetic regulation and transcription termination. *Genome Res* 23: 1590 – 1600

Gomez-Gonzalez B, Garcia-Rubio M, Bermejo R, Gaillard H, Shirahige K, Marin A, Foiani M, Aguilera A (2011) Genome-wide function of THO/TREX in active genes prevents R-loop-dependent replication obstacles. *EMBO J* 30: 3106 – 3119

Gong J, Traganos F, Darzynkiewicz Z (1994) A selective procedure for DNA extraction from apoptotic cells applicable for gel electrophoresis and flow cytometry. *Anal Biochem* 218: 314 – 319

Groh M, Lufino MM, Wade-Martins R, Gromak N (2014) R-loops associated with triplet repeat expansions promote gene silencing in *Friedreich ataxia* and fragile X syndrome. *PLoS Genet* 10: e1004318

Grzenda A, Lomberk G, Zhang JS, Urrutia R (2009) Sin3: master scaffold and transcriptional corepressor. *Biochim Biophys Acta* 1789: 443 – 450

Halazonetis TD, Gorgoulis VG, Bartek J (2008) An oncogene-induced DNA damage model for cancer development. *Science* 319: 1352 – 1355

Hamperl S, Cimprich KA (2014) The contribution of co-transcriptional RNA:DNA hybrid structures to DNA damage and genome instability. *DNA Repair* 19: 84 – 94

Hatchi E, Skourti-Stathaki K, Ventz S, Pinello L, Yen A, Kamieniarz-Gdula K, Dimitrov S, Pathania S, McKinney KM, Eaton ML, Kellis M, Hill SJ, Parmigiani G, Proudfoot NJ, Livingston DM (2015) BRCA1 recruitment to transcriptional pause sites is required for R-loop-driven DNA damage repair. *Mol Cell* 57: 636 – 647

Hecht A, Grunstein M (1999) Mapping DNA interaction sites of chromosomal proteins using immunoprecipitation and polymerase chain reaction. *Methods Enzymol* 304: 399 – 414

Hegele A, Kamburov A, Grossmann A, Sourlis C, Wowro S, Weimann M, Will CL, Pena V, Luhrmann R, Stelzl U (2012) Dynamic protein-protein interaction wiring of the human spliceosome. *Mol Cell* 45: 567 – 580

Herrera-Moyano E, Mergui X, Garcia-Rubio ML, Barroso S, Aguilera A (2014) The yeast and human FACT chromatin-reorganizing complexes solve R-loop-mediated transcription-replication conflicts. *Genes Dev* 28: 735 – 748

Hodroj D, Recolin B, Serhal K, Martinez S, Tsanov N, Abou Merhi R, Maiorano D (2017) An ATR-dependent function for the Ddx19 RNA helicase in nuclear R-loop metabolism. *EMBO J* 36: 1182 – 1198

Huertas P, Aguilera A (2003) Cotranscriptionally formed DNA:RNA hybrids mediate transcription elongation impairment and transcription-associated recombination. *Mol Cell* 12: 711 – 721

Jelinic P, Pellegrino J, David G (2011) A novel mammalian complex containing Sin3B mitigates histone acetylation and RNA polymerase II progression within transcribed loci. *Mol Cell Biol* 31: 54 – 62

Jimeno S, Luna R, Garcia-Rubio M, Aguilera A (2006) Tho1, a novel hnRNP, and Sub2 provide alternative pathways for mRNP biogenesis in yeast THO mutants. *Mol Cell Biol* 26: 4387 – 4398

Kadamb R, Mittal S, Bansal N, Batra H, Saluja D (2013) Sin3: insight into its transcription regulatory functions. *Eur J Cell Biol* 92: 237 – 246

Li X, Manley JL (2005) Inactivation of the SR protein splicing factor ASF/SF2 results in genomic instability. *Cell* 122: 365 – 378

Li X, Niu T, Manley JL (2007) The RNA binding protein RNPS1 alleviates ASF/SF2 depletion-induced genomic instability. *RNA* 13: 2108 – 2115

Luna R, Rondon AG, Aguilera A (2012) New clues to understand the role of THO and other functionally related factors in mRNP biogenesis. *Biochim Biophys Acta* 1819: 514 – 520

Madireddy A, Kosiyatrakul ST, Boisvert RA, Herrera-Moyano E, Garcia-Rubio ML, Gerhardt J, Vuono EA, Owen N, Yan Z, Olson S, Aguilera A, Howlett NG, Schildkraut CL (2016) FANCD2 facilitates replication through common fragile sites. *Mol Cell* 64: 388 – 404

Paulsen RD, Soni DV, Wollman R, Hahn AT, Yee MC, Guan A, Hesley JA, Miller SC, Cromwell EF, Solow-Cordero DE, Meyer T, Cimprich KA (2009) A genome-wide siRNA screen reveals diverse cellular processes and pathways that mediate genome stability. *Mol Cell* 35: 228 – 239

Pile LA, Wassarman DA (2000) Chromosomal localization links the SIN3-RPD3 complex to the regulation of chromatin condensation, histone acetylation and gene expression. *EMBO J* 19: 6131 – 6140

Santos-Pereira JM, Aguilera A (2015) R loops: new modulators of genome dynamics and function. *Nat Rev Genet* 16: 583 – 597

Sanz LA, Hartono SR, Lim YW, Steyaert S, Rajpurkar A, Ginno PA, Xu X, Chedin F (2016) Prevalent, dynamic, and conserved R-loop structures associate with specific epigenomic signatures in mammals. *Mol Cell* 63: 167 – 178

Schwab RA, Nieminuszczy J, Shah F, Langton J, Lopez Martinez D, Liang CC, Cohn MA, Gibbons RJ, Deans AJ, Niedzwiedz W (2015) The fanconi anemia pathway maintains genome stability by coordinating replication and transcription. *Mol Cell* 60: 351 – 361

Shahbazian MD, Grunstein M (2007) Functions of site-specific histone acetylation and deacetylation. *Annu Rev Biochem* 76: 75 – 100

Silverstein RA, Ekwall K (2005) Sin3: a flexible regulator of global gene expression and genome stability. *Curr Genet* 47: 1 – 17

Skourti-Stathaki K, Proudfoot NJ, Gromak N (2011) Human senataxin resolves RNA/DNA hybrids formed at transcriptional pause sites to promote Xrn2-dependent termination. *Mol Cell* 42: 794 – 805

Skourti-Stathaki K, Proudfoot NJ (2014) A double-edged sword: R loops as threats to genome integrity and powerful regulators of gene expression. *Genes Dev* 28: 1384 – 1396

Skourti-Stathaki K, Kamieniarz-Gdula K, Proudfoot NJ (2014) R-loops induce repressive chromatin marks over mammalian gene terminators. *Nature* 516: 436 – 439

Smith KT, Martin-Brown SA, Florens L, Washburn MP, Workman JL (2010) Deacetylase inhibitors dissociate the histone-targeting ING2 subunit from the Sin3 complex. *Chem Biol* 17: 65 – 74

Soderberg O, Gullberg M, Jarvius M, Ridderstrale K, Leuchowius KJ, Jarvius J, Wester K, Hydbring P, Bahram F, Larsson LG, Landegren U (2006) Direct observation of individual endogenous protein complexes *in situ* by proximity ligation. *Nat Methods* 3: 995 – 1000

Sollier J, Cimprich KA (2015) Breaking bad: R-loops and genome integrity. *Trends Cell Biol* 25: 514 – 522

Sridhara SC, Carvalho S, Grosso AR, Gallego-Paez LM, Carmo-Fonseca M, de Almeida SF (2017) Transcription dynamics prevent RNA-mediated genomic instability through SRPK2-dependent DDX23 phosphorylation. *Cell Rep* 18: 334 – 343

Stirling PC, Chan YA, Minaker SW, Aristizabal MJ, Barrett I, Sipahimalani P, Kobor MS, Hieter P (2012) R-loop-mediated genome instability in mRNA cleavage and polyadenylation mutants. *Genes Dev* 26: 163 – 175

Tuduri S, Crabbe L, Conti C, Tourriere H, Holtgreve-Grez H, Jauch A, Pantesco V, De Vos J, Thomas A, Theillet C, Pommier Y, Tazi J, Coquelle A, Pasero P (2009) Topoisomerase I suppresses genomic instability by preventing interference between replication and transcription. *Nat Cell Biol* 11: 1315 – 1324

Vijayraghavan S, Tsai FL, Schwacha A (2016) A checkpoint-related function of the MCM replicative helicase is required to avert accumulation of RNA:DNA hybrids during S-phase and ensuing DSBs during G2/M. *PLoS Genet* 12: e1006277

Wahba L, Amon JD, Koshland D, Vuica-Ross M (2011) RNase H and multiple RNA biogenesis factors cooperate to prevent RNA:DNA hybrids from generating genome instability. *Mol Cell* 44: 978 – 988

Wahba L, Costantino L, Tan FJ, Zimmer A, Koshland D (2016) S1-DRIP-seq identifies high expression and polyA tracts as major contributors to R-loop formation. *Genes Dev* 30: 1327 – 1338

Wellinger RE, Prado F, Aguilera A (2006) Replication fork progression is impaired by transcription in hyperrecombinant yeast cells lacking a functional THO complex. *Mol Cell Biol* 26: 3327 – 3334

Yoshida M, Kijima M, Akita M, Beppu T (1990) Potent and specific inhibition of mammalian histone deacetylase both *in vivo* and *in vitro* by trichostatin A. *J Biol Chem* 265: 17174 – 17179